Production, characterization and testing of antibacterial PVA membranes loaded with HA-Ag$_3$PO$_4$ nanoparticles, produced by SC-CO$_2$ phase inversion

Short title: Production and testing of antibacterial PVA membranes produced by SC-CO$_2$ process

Lucia Baldino[1], Javier Aragón[2], Gracia Mendoza[2], Silvia Irusta[2,*], Stefano Cardea[1,*], Ernesto Reverchon[1]

[1] *Department of Industrial Engineering, University of Salerno, Via Giovanni Paolo II, 132, 84084 Fisciano (SA), Italy*

[2] *Nanoscience Institute of Aragon (INA) and Networking Biomedical Research Center of Bioengineering, Biomaterials and Nanomedicine (CIBER-BBN), 50018, Zaragoza, Spain; Aragon Health Research Institute (IIS Aragon), 50009, Zaragoza, Spain*

Corresponding authors information:

sirusta@unizar.es; +34876555437; www.unizar.es/nfp (Silvia Irusta)

scardea@unisa.it; +39089964091; www.supercriticalfluidgroup.unisa.it (Stefano Cardea)

Abstract

BACKGROUND: Silver loaded hydroxyapatite nanoparticles were incorporated into poly(vinyl alcohol) (PVA) membranes obtained by supercritical CO_2 (SC-CO_2) assisted phase inversion. Ag_3PO_4 crystals of 2.2±0.6 nm were dispersed in synthesized needle-like hydroxyapatite nanoparticles (20x65 nm) and were uniformly deposited on the internal surfaces of the PVA membranes. Operative conditions to produce membranes by SC-CO_2, PVA concentration and the effect on membranes porosity and morphology were studied.

RESULTS: Solutions at 20% w/w PVA produced membranes with cellular morphology and nanoporous walls; whereas, 30 and 50% w/w solutions produced nanostructured membranes. Silver ions were released from PVA membranes mainly by diffusion according to Peppas-Sahlin model. Membranes obtained at 20% w/w PVA showed a significant *E. coli* inhibition at an Ag concentration of 9 ppm, reaching the Minimal Inhibitory Concentration (MIC) and improving the bactericidal activity of the nanoparticles.

CONCLUSION: A concentration of Ag_3PO_4 crystals of about 22 ppm was calculated as capable to completely destroy these bacteria, reaching the Minimum Bactericidal Concentration (MBC).

1. Introduction

A large interest in the generation of polymeric structures characterized by antimicrobial properties has been developed in several fields, such as food engineering (i.e., active packaging), biomedical applications (i.e., wound dressing) and tissue engineering (i.e., scaffolds). The possibility of using biodegradable/biocompatible structures is a relevant goal to prolong and to control the release of antibacterial compounds. In order to achieve this objective, a desired property of antibacterial materials is to assure at least the Minimum Inhibitory Concentration (MIC); i.e., the minimum concentration that blocks bacteria proliferation on the target microorganisms and possibly to obtain the Minimum Bactericidal Concentration (MBC), related to the complete elimination of bacteria.

Several authors produced composite polymeric materials loaded with active agents, such as silver [1-3] and enzymes.[4,5] In particular, silver (Ag) exerts disinfectant and antibacterial activities, due to the bonds that its ions establish with the bacterial cell wall and cell membrane, inhibiting the respiration process.[6,7] An alternative to the use of Ag nanoparticles alone, is their adsorption on ceramic supports to avoid nanoparticles agglomeration and to control their release against the target microorganisms. For example, Miranda et al.[6] used a colloidal chemical route and a subsequent chemical reduction process to produce silver-hydroxyapatite nanocomposites at 1% w/w of metallic silver. They tested the antimicrobial activity of these nanocomposites against *Escherichia coli* and *Micrococcus luteus*, obtaining a completely disinfection.

Hydroxyapatite (HA) is generally selected as support for silver nanoparticles since it is biocompatible and suitable for medical applications.[8,9] Mocanu et al.[7] prepared nano-HA doped with zinc (0.2% w/w), silver (0.25% w/w) and gold (0.025% w/w), by an innovative wet chemical approach, coupled with a reduction process for silver and gold. These composite nanoparticles had a mean diameter of 70 nm; their antibacterial activity against *E. coli, Staphylococcus aureus, Staphylococcus spp., Bacillus cereus* and *Candida albicans* was investigated, revealing that the antimicrobial effect increased with the Ag nanoparticles content in the composites.

Polyvinyl alcohol (PVA) is one of the best candidates among synthetic polymers to be loaded with active nanoparticles, since it is biodegradable, biocompatible, non-toxic, non-carcinogenic and shows swelling properties and bio-adhesive characteristics.[10] Hong et al.[11] produced PVA nanofibers containing Ag nanoparticles by electrospinning; their antimicrobial activity was tested against *S. aureus* and *Klebsiella pneumoniae*, obtaining a colonies reduction larger than 99.9% after 18 h of incubation. Yu et al.[12] prepared poly(vinyl alcohol)/poly(N-vinyl pyrrolidone) hydrogels by freeze drying containing silver nanoparticles as potential wound dressing. The silver content in the aerogel was in the range of 0.1-1.0% w/w and silver particle size ranged from 20 to 100 nm. However, an irregular porous morphology of the composite aerogels was observed.

Traditional polymeric membrane formation processes show several limitations: reduced flexibility in controlling membrane morphology, long processing time and the membranes have to be accurately cleaned to eliminate organic solvents used during the formation process. Supercritical CO_2 (SC-CO_2) assisted phase inversion has been proposed to improve membranes production of several polymers,[13-18] that in some cases were loaded with pharmaceuticals,[13] catalysts [14] and active agents [15] for biomedical and food applications. Using this green technique, in a fast process and directly eliminating the organic solvent, membranes characterized by a regular and homogeneous micro and nanoporous morphology were produced, that is one of the key requirements for controlled release systems.[15,19] These results are due to the peculiar characteristics of CO_2 at supercritical conditions: high solvent power and high diffusivities, that allow an efficient control of membrane morphology; low surface tension, that avoids the collapse of the polymeric structure during the formation process. However, until now, SC-CO_2 assisted phase inversion has been applied only in some cases to the formation of loaded membranes and has never been applied to the formation of PVA membranes loaded with HA-Ag nanocomposites.

Therefore, in the present work, the production of PVA membranes loaded with HA-Ag nanoparticles by SC-CO_2 assisted phase inversion, for antibacterial applications, is proposed for the first time. First, the synthesis of hydroxyapatite/silver phosphate nanoparticles was performed; then,

these nanoparticles were loaded in the PVA membranes. PVA membranes, alone and loaded with the nanocomposite particles, were characterized from a physico-chemical point of view; in particular, the following analyses were performed: scanning electron microscopy (SEM), energy-dispersive X-ray spectroscopy (EDX), transmission electron microscopy (TEM), differential scanning calorimetry (DSC), nitrogen adsorption, Hg-porosimetry, X-ray diffraction (XRD), thermogravimetric analysis (TGA) and plasma atomic emission spectrometry (MP-AES). Moreover, bactericidal activity against a model bacteria (*E. coli)* was tested, determining MIC and MBC. Ag release study was performed and modelled using Korsmeyers-Peppas and Peppas-Sahlin equations in order to verify their applicability to the results of this study.

2.   Materials and methods

2.1   Materials

Polyvinyl alcohol (PVA, M_w 31.000-50.000; 98-99% hydrolyzed), dimethyl sulfoxide (DMSO, purity >99.5%), calcium carbonate ($CaCO_3$), phosphoric acid (H_3PO_4) and silver nitrate ($AgNO_3$) were bought from Sigma-Aldrich. CO_2 (purity 99.9%) was supplied by Morlando Group s.r.l. (Sant'Antimo, NA - Italy). All materials were processed as received.

2.2   Synthesis of HA nanoparticles

The synthesis of hydroxyapatite nanoparticles, with needle-like morphology, was carried out using a modification of the Wet Chemical Precipitation,[20] that uses $CaCO_3$ as the calcium source. $CaCO_3$ was added to a solution of H_3PO_4 to obtain a Ca/P ratio of 1.67. pH of the solution was adjusted between 3 and 4 adding HCl in order to dissolve all $CaCO_3$; after that, the solution was left under stirring for 6 h at room temperature. The precipitation of hydroxyapatite was performed by a dropwise addition of NH_4OH, bringing the solution to a pH greater than 9. The solution was placed in an oil bath for 1-2 h at 100 °C; then, it was centrifuged at 13000 rpm for 15 min and washed

several times with distilled water to obtain pH=7 and, at the end, it was washed with ethanol, centrifuged again and placed to dry at 100 °C for 24 h.

2.3 Synthesis of HA nanoparticles loaded with Ag₃PO₄ nanoparticles

The synthesis of composite particles of hydroxyapatite and $AgNO_3$, was performed as described in the literature.[21] HA nanoparticles were mixed with an $AgNO_3$ solution, with an HA/Ag weight ratio of 20:1. The mixture was kept under constant stirring at room temperature for 2 h and then centrifuged; the pellet was dried at 60 °C for 72 h. The obtained particles are mentioned as HA-Ag.

2.4 PVA membranes preparation procedure

PVA was dissolved by magnetic stirring in DMSO for 12 h at room temperature. When an homogeneous solution was obtained, nanoparticles at 15% w/w with respect to the polymer were added. The suspension was mixed by Vortex and rapidly distributed on stainless steel caps of 2 cm diameter and 800 μm height and, finally, processed by SC-CO_2 phase inversion.

A home-made high pressure laboratory plant was used, that has been described elsewhere.[22] The caps were put inside an high pressure vessel (a 316 stainless steel vessel with an internal volume of 200 mL); it was closed and filled with CO_2 up to the operative pressure, using an high pressure pump (mod. LDB1, Lewa, Germany). Then, samples were processed by SC-CO_2 phase inversion at different process conditions and each run lasted 5 h. Pressure in the vessel was measured by a test gauge (mod. MP1, OMET, Italy) and regulated using a micrometering valve (mod. 1335G4Y, Hoke, USA). Temperature was regulated using PID controllers (mod. 305, Watlow, USA). At the exit of the vessel, a rotameter (mod. D6, ASA, Italy) was used to measure the CO_2 flow rate, that was maintained constant at 1.5 kg/h.

2.5   Characterization techniques

2.5.1   *Scanning electron microscopy (SEM)*

PVA membranes were cryo-fractured using liquid nitrogen (SOL, Milan, Italy); then, samples were sputter coated with gold (Agar Auto Sputter Coater mod. 108 A, Stansted, UK) at 30 mA for 120 s and analyzed by a SEM (mod. LEO 1525, Carl Zeiss SMT AG, Oberkochen, Germany) to study the membrane morphology. A Field Emission Scanning Electron Microscope (CSEM-FEG INSPECT 50, FEI, USA) was used to study the HA particles morphology.

SEM assays were performed in *E. coli,* following the methodology previously described.[23] Briefly, bacteria (10^7 CFU/mL) were centrifuged and re-suspended in HA-Ag nanoparticles at MIC and at a higher concentration. After incubation (37 °C; 24 h), bacteria were washed in a Phosphate Buffered Saline (PBS) solution 0.1 M and fixed in glutaraldehyde (2.5%; 90 min). Finally, samples were filtered and dehydrated in ethanol series to be further air-dried and coated with a thin Pt layer; the images were recorded using a SEM (Inspect F50, FEI Co., LMA-INA, Spain) in an energy range between 10 and 15 keV.

2.5.2   *Transmission electron microscopy (TEM)*

Morphology, size and distribution of silver particles supported on HA were analyzed using a transmission electron microscope (TEM) operated at 300 kV (Tecnai F30, FEI, USA) and a JEOL-2000 FXII transmission electron microscope (JEOL, Japan) equipped with a Tecnai T20 thermionic LaB_6 filament, at 200 kV. The size distribution statistics were obtained by measuring at least 100 particles in different images. The energy-dispersive (EDX) mapping was used to analyze the composition of materials.

2.5.3   *Differential scanning calorimetry (DSC)*

DSC (DSC 30 Mettler, Toledo, Spain) was carried out to analyze and identify any changes in the thermograms of pure substances compared to polymer/nanoparticles formulations. Calorimetric

analysis was performed in the temperature range between 25 and 300 °C, with an heating rate of 10 °C/min; the inert gas was nitrogen, with a flow rate of 50 L/min.

2.5.4 Nitrogen adsorption

BET specific surface area was determined by N_2 physisorption using a Nova 1200e Surface Area & Pore Size Analyzer (Quantachrome Instruments, Florida, USA). 0.1-0.2 g of membrane sample were first degassed under vacuum at 40 °C for 12 h prior to the analysis followed by N_2 adsorption at -196 °C. BET analysis was carried out at a relative vapour pressure of 0.01-0.3 bar at -196 °C.

2.5.5 Hg-porosimetry

Mercury porosimetry experiments were performed using an automated mercury porosimeter (POREMASTER®, Quantachrome). The mercury volume intruded as a function of pressure was monitored in order to determine the pore size distributions. The tests were carried out in accordance with ISO 15901-1 standard.

2.5.6 X-ray diffraction (XRD)

The powder diffraction pattern of synthesized nanoparticles was measured in a diffractometer (Rigaku RINT 2000) with a monochromatic Cu Kα radiation.

2.5.7 Energy dispersive X-ray spectroscopy (EDX)

Loaded membranes were cryo-fractured using liquid nitrogen and sputter coated with chrome (EMITECH K575X peltier cooled); then, they were analyzed by energy dispersive X-ray spectroscopy (EDX) (INCA Energy 350, Oxford Instruments) in order to identify the elements forming the samples; in particular, Calcium atoms were selected for HA identification in the polymer matrix.

2.5.8 *Thermogravimetric analysis (TGA)*

In order to measure the membranes inorganic content, thermal analyses were conducted with a thermogravimetric analyzer (TGA/SDTA 851e, METTLER TOLEDO).

2.5.9 *Plasma atomic emission spectrometry (MP-AES)*

The bulk chemical composition of digested samples was analyzed using a microwave plasma atomic emission spectrometry (Agilent 4100 MP-AES). The solid samples were digested with 0.5 M of nitric acid for 1 h and analyzed in quintuplicate.

2.6   Antimicrobial activity test

The antimicrobial activity of a substance is measured by determining the lowest concentration of the substance required to inhibit the growth of a given microorganism (MIC) and the minimum bactericidal concentration (MBC). *E. coli S17* (10^5 CFU/mL) was the model microorganism selected in this study.

As the Ag content in the nanoparticles was fixed, the proper quantities of nanoparticles were used in a fixed volume of 4 mL of an overnight stationary growth phase bacteria in Tryptone Soy Broth (TSB) to reach the desired concentrations. The silver-containing materials were previously sterilized using ethanol vapors. Liquid cultures (TSB) were incubated at 37 °C for 24 h under shaking (150 rpm), while loaded PVA membranes were assayed in solid cultures samples (Tryptone Soy Agar, TSA) and incubated at the same conditions but without shaking. After incubation, samples were diluted (10^1-10^6) in duplicate and all dilutions were seeded on agar plates in triplicate. Viable bacterial colonies were counted after incubation overnight at 37 °C. Bacteria cultures non treated with Ag nanoparticles were used as control samples. All samples were run in duplicate.

2.7   Silver release tests

Silver ions *in vitro* release from membranes was determined by microwave plasma atomic emission spectrometry (Agilent 4100 MP-AES). Three samples per membrane were immersed in PBS for 24 h at 37 °C. According to scheduled time intervals (from 1, 2, 3, 4, 5, 6, 7, 8 and 24 h) all PBS was collected and replaced with an equal volume of fresh PBS. The linear range of the calibration curve for Ag(I) was 1.0-60.0 ppm.

Two different mathematical models were selected to represent the Ag release kinetics.

1) Korsmeyer and Peppas [24] derived a simple relationship that describes the release of a drug from a polymeric system as:

$$\frac{Ct}{C\infty} = k * t^n$$

where:

C_t/C_∞=fraction of drug released at time t

k=rate constant

n=release exponent

2) Similarly, Peppas and Sahlin [25] developed a two rate constants model:

$$\frac{Ct}{C\infty} = k1 * t^n + k2 * t^{2n}$$

where:

C_t/C_∞=fraction of drug released at time t

k_1, k_2=rate constant

n=release exponent

2.8   Statistical analysis

The results are expressed as mean ± SD (12 data per concentration and dilution). Normal distribution of the variables was analyzed by the Shapiro-Wilk test followed by the U-Mann-

Whitney, ANOVA or Student test (StataSE 12 statistical software, StataCorp LP, USA). Statistically significant differences among groups were considered when p ≤0.05.

3. Results and discussion

3.1 HA and HA-Ag nanoparticles

The size distribution of the HA nanoparticles was measured using SEM images, as for example in Figure 1a. They showed a length of about 65 nm and a thickness of about 20 nm; TEM images (Figure 1b) confirmed their morphology and structure. The needle-like shape of the nanoparticles was due to a preferred growth orientation along the c-axis.[26] SEM image in Figure 1c of HA-Ag composite shows that the needle-like morphology of hydroxyapatite nanoparticles was not altered by the presence of Ag and TEM image in Figure 1d shows a good dispersion and distribution of crystals above those of hydroxyapatite. According to the literature, silver impregnation of hydroxyapatite results in the deposition of Ag_3PO_4 nanoparticles on the support.[21] The size of these Ag_3PO_4 crystals was measured from TEM images (2.2±0.6 nm).

Silver load in the nanoparticles, measured by chemical analysis, was found to be 0.9±0.1% w/w, much lower than the theoretical one (5% w/w), showing that part of the silver nitrate was lost during the washing-centrifugation process.

Figure 1. a) SEM and b) TEM images of HA nanoparticles, c) SEM and d) TEM images of HA-Ag nanoparticles.

XRD patterns of HA and HA-Ag are shown in Figure 2; a good matching in terms of peak positions and peak intensities was observed by comparing the obtained XRD patterns with the standard. Broad and noisy peaks were due to samples small particles size and low crystallinity. In the HA-Ag pattern, peaks at 20.9, 29.7, 33.3 and 36.6º revealed the presence of crystalline Ag_3PO_4 (JCPDS 01-070-0702) indicating the Ag^+ lattice substitution for Ca^{2+} ions.[27]

Figure 2. XRD of a) HA-Ag, b) HA-Ag nanoparticles and c) HA standard.

3.2 PVA membranes

PVA was dissolved at different concentrations (20, 30 and 50% w/w) in DMSO, to produce membranes by phase inversion assisted by SC-CO$_2$. Different operative conditions were studied in order to determine the influence of SC-CO$_2$ density on membranes morphology in the range 35-55 °C and 150-250 bar. In particular, the selected p/T combinations were: 150/55, 200/45 and 250/35 bar/°C, corresponding to SC-CO$_2$ densities of 0.66, 0.81 and 0.90 g/cm^3, respectively.

At 150 bar and 55 °C, an irregular PVA membrane morphology was observed and PVA crystals were also found (Figure 3a). Probably, at the lowest SC-CO$_2$ density, the process kinetics were too slow and, during the process, PVA tended to precipitate as crystals, since it had time to re-organize its structure. Membranes produced at 200 bar and 45 °C (Figure 3b) and 250 bar and 35 °C (Figure 3c), instead, showed a porous morphology; as a consequence, the attention was focused on 200 bar and 45 °C for further processing, identified as a good compromise between porous morphology suitable to accommodate the nanoparticles and process intensity. In Table 1, the codes used in this work are reported, to identify the polymeric membranes.

Figure 3. SEM images of PVA20: a) 150 bar, 55 °C; b) 200 bar, 45 °C; c) 250 bar, 35 °C.

Table 1. Codes of the produced membranes and specific area results.

DSC thermograms of untreated PVA and of PVA membranes were compared. The polymer, after supercritical processing, preserved its T$_m$ at about 225 °C and its T$_g$ at about 75 °C, as evidenced in Figure 4a-b. Therefore, the supercritical process did not affect the physico-chemical properties of the polymer.

Figure 4. DSC of (a) untreated PVA and (b) PVA20 membrane.

SEM images reported in Figure 5a-c are related to the cross sections of the PVA membranes loaded with 15% w/w HA with respect to the polymer, obtained by SC-CO_2 processing at 200 bar and 45 °C: PVA30-HA (Figure 5b) and PVA50-HA (Figure 5c) membranes were more compact with respect to PVA20-HA (Figure 5a) and characterized by a nanofilamentous structure.

Figure 5. SEM images of: a) PVA20-HA, b) PVA30-HA and c) PVA50-HA membranes, obtained at 200 bar and 45 °C.

In Table 1, BET results for PVA membranes loaded with HA are reported. The specific surface area decreased, increasing PVA concentration in the membrane; this result is compatible with what it has been previously shown by SEM images (Figure 5a-c). In particular, the structure of membranes at larger PVA concentrations was closer and compact, passing from a cellular structure (with nanometric substructure) to a thick nanoporous network, with a consequent decrease of the specific area.

At this point of the work, PVA membranes were loaded with HA-Ag nanoparticles (HA/Ag ratio 20/1) again at 15% w/w with respect to the polymer. In order to obtain an effective suspension of the nanoparticles, a Vortex dispersion system was used to prepare the suspensions of HA-Ag nanoparticles in the PVA/DMSO solutions, as explained in Materials and Methods. The suspensions were rapidly processed by supercritical phase inversion to avoid nanoparticles re-aggregation.

The thermograms of PVA-HA and PVA-HA-Ag membranes were produced to detect possible differences in their thermal behaviour. No variations were found; loaded membranes maintained the characteristic temperatures of PVA alone membranes: $T_g \cong 75$ °C and $T_m \cong 225$ °C.

SEM images of PVA-HA and PVA-HA-Ag membranes were similar (Figure 6); i.e., the morphology previously observed for PVA-HA membranes (Figure 5a-b) was maintained. But, they also showed the nanoparticles covering the underlying polymeric structure that was still porous. This detail is particularly evident when higher SEM enlargements are used, like in Figure 6b.

Figure 6. SEM images of a) - b) PVA20-HA-Ag and c) PVA30-HA-Ag membranes, obtained at 200 bar and 45 °C.

PVA20-HA-Ag membranes maintained the cellular morphology (Figure 6a), observed in the case of PVA membranes (Figure 3b); but, nanoporous walls were covered by nanoparticles, as evidenced at larger magnifications (Figure 6b). Figure 6c shows that PVA30-HA-Ag membranes presented again the nano-filamentous structure with interconnected and elongated fibers; nanoparticles were intercalated within the polymer matrix. PVA50-HA-Ag membrane was characterized by a more compact structure, in which the nanoparticles precipitated on the underlying matrix. EDX analyses were also performed, in order to observe the HA-Ag distribution along the PVA membranes; at all operative conditions, an homogeneous distribution of the nanoparticles in the membranes section was obtained. For example, in Figure 7, the EDX map of Calcium (i.e., HA-Ag nanoparticles distribution) in PVA20-HA-Ag membrane section is reported. Moreover, we also evidenced as the part of HA-Ag nanoparticles that was not embedded in the polymeric matrix (i.e., present on membranes skins) can be considered negligible.

Figure 7. EDX map of HA-Ag nanoparticles in a PVA20-HA-Ag membrane.

Due to the morphology of PVA50-HA-Ag membranes and to the difficulty in treating the very viscous starting solution, it was decided to continue the processing of the PVA20-HA-Ag and PVA30-HA-Ag only, on which TGA analysis and bactericidal tests were performed.

TGA analysis showed a content of loaded nanoparticles between 18 and 16% w/w, respectively, compared to the total membrane weight, as reported in Figure 1SI (Supplementary material). Therefore, the experimental result was very close to theoretical nanoparticles content of 15% w/w of the polymer.

Hg porosimetry performed on the PVA20-HA-Ag and PVA30-HA-Ag membranes, evidenced that PVA20-HA-Ag sample showed two size populations: a first one ranging from 20 to 30 μm (i.e., cellular structure) and a second one ranging from 20 to 40 nm (i.e., nanoporous sub-structure); these results are reported in Figure 2SIa (Supplementary material). The mean values were measured in correspondence of the inflection point of each interval on the curve and resulted about 25 μm and 30 nm. In PVA30-HA-Ag membrane, pores ranged from 200 nm and 300 nm and the mean value was about 250 nm (see Figure 2SIb, Supplementary material). Moreover, PVA20-HA-Ag membrane had a porosity of about 88%; whereas, the PVA30-HA-Ag porosity was of about 78%.

3.3   Silver release from PVA membranes

Ag release study was performed on PVA20-HA-Ag and PVA30-HA-Ag membranes, with the aim of calculating the membrane mass (i.e., Ag concentration in a fixed quantity of culture medium) necessary to achieve the MBC during bactericidal tests.[28] In Figure 8a-b, Ag release is plotted in terms of Ag concentration and percentage of Ag released. The cumulative release for PVA20-HA-Ag membranes was larger than that of PVA30-HA-Ag in 24 h testing. The first one released around 43.5% of the total loaded Ag and 30.5% after 8 h. PVA30-HA-Ag, instead, released only 13.7% Ag during the first 8 h and 27.2% after 24 h. A possible explanation of these results is related to the different membrane morphologies: cellular and nanoporous, for PVA20-HA-Ag and PVA30-HA-Ag, respectively. Nanoporous morphology limited the Ag diffusion along the polymeric structure, reducing silver release; whereas, a cellular structure promoted silver ions diffusion due to the larger pores and surface area. In addition, nanoparticles in the PVA20-HA-Ag membrane were arranged on the pores wall and not in the polymer matrix, favoring ions release.

Figure 8. a) - b) Ag release from PVA20-HA-Ag and PVA30-HA-Ag plotted in terms of a) amount of Ag released and b) % of Ag released during 24 h; c) - d) comparison of the fitting models: c) PVA30-HA-Ag (Korsmeyers-Peppas: blu, Peppas-Sahlin: red) and d) PVA20-HA-Ag (Korsmeyers-Peppas: blu, Peppas-Sahlin: red) membranes during the first 8 h of release.

Several mathematical models have been proposed in the literature to describe active principles release from polymeric matrices. Among them, in this work Korsmeyer-Peppas and Peppas-Sahlin were selected in order to describe the Ag release from the PVA membranes. The calculations were limited to the first 8 h, since one of the assumptions of these models is that they are applicable for short release times.[29] The results obtained (adjusted-R^2) as well as their respective constants are shown in Figure 8c-d and Table 2. In the case of PVA30-HA-Ag (Figure 8c), the two models curves completely overlapped.

Table 2. Fitting parameters of Korsmeyers-Peppas model on PVA20-HA-Ag and PVA30-HA-Ag membranes.

In the Korsmeyer-Peppas model, k value is related to the ratio between diffusion and membrane tortousity. Figure 6 shows that PVA30-HA-Ag (i.e., nanofilamentous morphology) had an higher tortuosity with respect to PVA20-HA-Ag (i.e., cellular morphology): for this reason, it is reasonable that k value for PVA30-HA-Ag membranes is lower than the value found for PVA20-HA-Ag membranes. Moreover, the release exponent n of this model describes different release mechanisms from the solid matrices; a value between 0.45 and 0.89 implies that the Ag release is controlled by a combination of diffusion and polymer relaxation. This result is consistent with the fact that PVA is an hydrosoluble polymer and during Ag release test it would show a relaxation process.

Substituting the n parameter obtained by Korsmeyer-Peppas model in the Peppas-Sahlin model, it is possible to find k_1 and k_2; the ratio k_1/k_2 is useful to determine the release controlling mechanism. For k_1/k_2 values larger than 1, the release is dominated mainly by Fickian diffusion; if the ratio is lower than 1, the active agent release is determined mainly by polymer chains relaxation.[29,30] For both membranes, Peppas-Sahlin model suggested that the predominant release mechanism was the diffusion of Ag ions. It is interesting to note that k_1/k_2 ratio was larger for PVA30-HA-Ag membranes; in this material, the polymer relaxation would be less relevant than for PVA20-HA-Ag membranes. This fact was probably related to the nanofilaments morphology (PVA30-HA-Ag) that tended to create chain entanglement.

3.4   Antimicrobial activity

In the literature it has been established that Ag_3PO_4 produces tunable Ag release rates, that give antibacterial activity by Ag ions release in biological fluids.[27] The antimicrobial activity against *E. coli* was studied for HA nanoparticles, as a control, and different amounts of Ag loaded nanoparticles were dispersed in TSB. The amount of particles was calculated to obtain Ag theoretical concentrations of 1.8, 3.6, 5.4, 7.2 and 9.0 ppm. The results of bactericidal tests for nanoparticles alone are shown in Figure 9.

Figure 9. Bactericidal activity of HA-Ag nanoparticles at different concentrations on *E. coli* cultures after 24 h.

Even at the lowest concentration, *E. coli* was affected by HA-Ag nanoparticles, showing a reduction of two logarithms and reaching MIC; in order to avoid misleading, this value will be indicated in the following of this paper as MIC_A, where A means that this value is referred to nanoparticles alone. Increasing the Ag concentration to 9 ppm, bacteria were completely destroyed obtaining MBC that, for the same reasons previously indicated, will be referred in the following as

MBC$_A$. SEM images for *E. coli* at nanoparticles concentrations of 1.8 and 5.4 ppm, indicate the bactericidal mechanism of the material (Figure 10). Untreated bacteria were characterized by a rod-like shape with smooth cell wall surface (Figure 10A-B). On the contrary, cell membrane damage exerted by Ag ions was clear in SEM images of Figure 10C-F, showing a wrinkled morphology together with damages in bacteria outer membrane. Accumulations of Ag nanoparticles were also observed in these images; their composition was checked by EDX.

Figure 10. SEM images of A) and B) untreated, treated with C) and D) 1.8 ppm and E) and F) 5.4 ppm suspensions of HA-Ag nanoparticles.

Subsequently, PVA20-HA-Ag membranes were assayed against *E. coli* in liquid and in solid cultures (Figure 11); in the latter case, bacteria growth was calculated from the whole culture and also in a 1 cm^2 area around the membrane. Bacteria cultures without the addition of membranes (CONTROL) and with the addition of unloaded membranes (PVA20) were used as control samples. Membranes mass used in these tests was calculated in order to have loadings equal to MIC$_A$ (1.8 ppm) and MBC$_A$ (9.0 ppm), found for the HA-Ag particles alone (Figure 9).

Unloaded PVA membranes (PVA20) did not have any effect on bacterial growth in solid or liquid cultures, and the same was for membranes loaded with particle at MIC$_A$ (MIC$_A$PVA20). This result can be explained considering that PVA20 membranes released only about 40% of Ag during the first 24 h (Figure 8). As a consequence, MIC$_A$PVA20 released about 0.7 ppm of Ag in 24 h, not reaching the MIC$_A$ (i.e., 1.8 ppm).

When the silver content at MBC$_A$ was used (MBC$_A$PVA20), a relevant inhibition of bacterial growth was found, showing a decrease of around 10^4 CFU/mL for the solid culture and an higher value ($\sim$10^6 CFU/mL) in the liquid culture. As above, taking into account that when the Ag load was 9 ppm (MBC$_A$PVA20), membranes released only about 40% of Ag during the first 24 h, the effective concentration faced by the bacteria was around 3.6 ppm. Then, it is possible to compare

this result with the one obtained for HA-Ag nanoparticles alone (Figure 9). Indeed, starting from the same Ag concentration (3.6 ppm), it was found that, for liquid culture, HA-Ag nanoparticles alone lead to a decrease of bacterial growth of about 10^3 CFU/mL in 24 h (3.6 ppm in Figure 9); whereas, HA-Ag nanoparticles loaded in the PVA20 membranes showed a decrease of 10^6 CFU/mL (MBC_APVA20 in Figure 11). This is a very interesting result: it evidences that loading of HA-Ag nanoparticles in PVA membranes strongly affected the nanoparticles bactericidal activity, that appeared to be two times stronger. The morphology of the polymeric support, allowed an increase of Ag nanoparticles on the exposed surface and, as a consequence, of their killing bacteria efficiency. However, in the hypothesis that the percentage of Ag ions released from PVA20 membrane was the same (40% in 24 h), this calculation suggests for PVA20 membranes, that a concentration of Ag nanoparticles of about 22 ppm should be enough to reach MBC_A, independently on nanoparticles bactericidal efficiency. Indeed, testing a suitable mass of PVA20 membrane containing 22 ppm of Ag, it should release about 9 ppm of Ag in 24 h (i.e., MBC_A). If the increase of nanoparticles bactericidal activity (i.e., two times stronger) would be confirmed, an Ag content of about 11 ppm could be sufficient for reaching MBC in 24 h. Moreover, for solid samples testing, when the area around the inhibition zone was collected, also the MIC_A sample (MIC_APVA20) exerted significant differences vs control samples. The difference between the results of the two procedures (solid culture vs solid culture-1 cm^2), highlights the importance of the contact between bacteria and membranes to obtain the inhibitory effects. This observation was confirmed by the analysis of 1 cm^2 around the membrane; it showed that when cells were in close contact with the membrane, even at MIC_A concentration, there was an inhibition of the bacterial growth.

Figure 11. Bactericidal results for PVA20-HA-Ag membranes against *E. coli* solid culture, liquid culture and the solid culture collection of 1 cm^2 around the membrane, for 24 h experiments.

4.   Conclusions and perspectives

PVA membranes loaded with HA-Ag nanoparticles have been successfully produced and PVA 20% w/w concentration has been selected due to the corresponding membrane morphology, that has been demonstrated to be the most suitable to host the active nanoparticles. Silver ions release from PVA membranes has been studied and modelled and it has been demonstrated that the key action of silver ions is to damage bacteria external membrane by direct contact.

HA-Ag nanoparticles loaded in PVA membranes were more active than the nanoparticles alone: probably, due to an increase of the exposed surface. Bacteria killing experiments, on 24 h duration, demonstrated that an Ag concentration of about 22 ppm should be enough to reach MBC for *E. coli*. But, if the entity of the increase of nanoparticles bactericidal activity found during the experimentations would be confirmed, an Ag content of only 11 ppm could be sufficient for reaching MBC; further studies will be performed to verify this hypothesis.

In any case, the final aim of this study has been successfully reached, obtaining a prolonged and controlled release of active Ag ions, that was the major drawback of using Ag nanoparticles alone. These membranes can be a promising material to avoid and defeat bacterial contamination in different applications. In particular, biomedical and coating applications are difficult due to the membranes morphology; but, water purification could be an interesting application. In any case, in a future work, we will focus our attention on the PVA-HA-Ag membranes applications, studying the HA-Ag release for longer time (i.e., longer than 24 h), the stability of the polymers and of the nanoparticles, the membranes permeability tests and the possibility to control the HA-Ag release acting on the physico-chemical characteristics of the membranes, for example adding a cross-linking agent to limit the PVA relaxation (i.e., to decrease Ag release rate).

References

1. Morones JR, Elechiguerra JL, Camacho A, Holt K, Kouri JB, Ramírez JT and Yacaman MJ, The bactericidal effect of silver nanoparticles. *Nanotechnol* **16**:2346 (2005).

2. Rhim JW, Wang LF and Hong SI, Preparation and characterization of agar/silver nanoparticles composite films with antimicrobial activity. *Food Hydrocolloids* **33**:327 (2013).

3. Fajardo AR, Lopes LC, Caleare AO, Britta EA, Nakamura CV, Rubira AF and Muniz EC, Silver sulfadiazine loaded chitosan/chondroitin sulfate films for a potential wound dressing application. *Mater Sci Eng C* **33**:588 (2013).

4. Charernsriwilaiwat N, Opanasopit P, Rojanarata T and Ngawhirunpat T, Lysozyme-loaded, electrospun chitosan-based nanofiber mats for wound healing. *Int J Pharm* **427**:379-384 (2012).

5. Piras AM, Maisetta G, Sandreschi S, Esin S, Gazzarri M, Batoni G and Chiellini F, Preparation, physical–chemical and biological characterization of chitosan nanoparticles loaded with lysozyme. *Int J Biol Macromol* **67**:124-131 (2014).

6. Miranda M, Fernández A, Díaz M, Esteban-Tejeda L, López-Esteban S, Malpartida F, Torrecillas R and Moya JS, Silver-hydroxyapatite nanocomposites as bactericidal and fungicidal materials. *Int J Mater Res* **101**:122-127 (2010).

7. Mocanu A, Furtos G, Rapuntean S, Horovitz O, Flore C, Garbo C, Danisteanu A, Rapuntean G, Prejmerean C and Tomoaia-Cotisel M, Synthesis; characterization and antimicrobial effects of composites based on multi-substituted hydroxyapatite and silver nanoparticles. *Appl Surf Sci* **298**:225-235 (2014).

8. Kantharia N, Naik S, Apte S, Kheur M, Kheur S and Kale B, Nano‑hydroxyapatite and its contemporary applications. *Bone* **34**:15-19 (2014).

9. Ciobanu CS, Iconaru SL, Pasuk I, Vasile BS, Lupu AR, Hermenean A, Dinischiotu A and Predoi D, Structural properties of silver doped hydroxyapatite and their biocompatibility. *Mater Sci Eng C* **33**:1395 (2013).

10. Baker MI, Walsh SP, Schwartz Z and Boyan BD, A review of polyvinyl alcohol and its uses in cartilage and orthopedic applications. *J Biomed Mater Res, Part B* **100**:1451-1457 (2012).

11. Hong KH, Park JL, Sul IH, Youk JH and Kang TJ, Preparation of antimicrobial poly (vinyl alcohol) nanofibers containing silver nanoparticles. *J Polym Sci, Part B: Polym Phys* **44**:2468-2474 (2006).

12. Yu H, Xu X, Chen X, Lu T, Zhang P and Jing X, Preparation and antibacterial effects of PVA-PVP hydrogels containing silver nanoparticles. *J Appl Polym Sci* **103**:125-133 (2007).

13. Cardea S, Baldino L, Scognamiglio M and Reverchon E, 3D PLLA/Ibuprofen composite scaffolds obtained by a supercritical fluids assisted process. *J Mater Sci: Mater Med* **25**:989-998 (2014).

14. Cardea S and Reverchon E, Nanostructured PVDF-HFP membranes loaded with catalyst obtained by supercritical CO_2 assisted techniques. *Chem Eng Process* **50**:630-636 (2011).

15. Baldino L, Cardea S and Reverchon E, Supercritical assisted enzymatic membranes preparation, for active packaging applications. *J Membr Sci* **453**:409-418 (2014).

16. Matsuyama H, Yano H, Maki T, Teramoto M, Mishima K and Matsuyama K, Formation of porous flat membrane by phase separation with supercritical CO_2. *J Membr Sci* **194**:157-163 (2001).

17. Huang S, Wu G and Chen S, Preparation of microporous poly(vinylidene fluoride) membranes via phase inversion in supercritical CO_2. *J Membr Sci* **293**:100-110 (2007).

18. Torres-Trueba A, Ruiz-Treviño FA, Luna-Bárcenas G and Ortiz-Estrada CH, Formation of integrally skinned asymmetric polysulfone gas separation membranes by supercritical CO_2. *J Membr Sci* **320**:431-435 (2008).

19. Cvjetko Bubalo M, Vidović S, Radojčić Redovniković I and Jokić S, Green solvents for green technologies. *J Chem Technol Biotechnol* **90**:1631-1639 (2015).

20. Paz A, Guadarrama D, López M, González JE, Brizuela N and Aragón J, A comparative study of hydroxyapatite nanoparticles synthesized by different routes. *Quim Nova* **35**:1724-1727 (2012).

21. Buckley JJ, Lee AF, Olivi L and Wilson K, Hydroxyapatite supported antibacterial Ag$_3$PO$_4$ nanoparticles. *J Mater Chem* **20**:8056-8063 (2010).

22. Baldino L, Cardea S and Reverchon E, Production of antimicrobial membranes loaded with potassium sorbate using a supercritical phase separation process. *Innovative Food Sci Emerging Technol* **34**:77-85 (2016).

23. Mendoza G, Regiel-Futyra A, Andreu V, Sebastian V, Kyziol A, Stochel G and Arruebo M, Bactericidal effect of gold-chitosan nanocomposites in coculture models of pathogenic bacteria and human macrophages. *ACS Appl Mater Interfaces* **9**:17693-17701 (2017).

24. Ritger P and Peppas N, A simple equation for description of solute release. *J Controlled Release* **5**:23-36 (1987).

25. Peppas NA and Sahlin JJ, A simple equation for the description of solute release .3. coupling of diffusion and relaxation. *Int J Pharm* **57**:169-172 (1989).

26. Aragon J, Navascues N, Mendoza G and Irusta S, Laser-treated electrospun fibers loaded with nano-hydroxyapatite for bone tissue engineering. *Int J Pharm* **525**:112-122 (2017).

27. Singh RP, Singh M, Verma G, Shukla S, Singh S and Singh S, Structural analysis of silver doped hydroxyapatite nanopowders by rietveld refinement. *Trans Indian Inst Met* **70**:1973-1980 (2017).

28. Dash S, Murthy PN, Nath L and Chowdhury P, Kinetic modeling on drug release from controlled drug delivery systems. *Acta Pol Pharm* **67**:217-223 (2010).

29. Liu J, Zu ZJ, Guo Z, Zhao ZG, Zhao Y and Wang X, Structural investigation of a polysaccharide from the mycelium of Enterobacter cloacae and its antibacterial activity against extensively drug-resistant E-cloacae producing SHV-12 extended-spectrum beta-lactamase. *Carbohydr Polym* **195**: 444-452 (2018).

30. Freire M, Alexandrino F, Marcelino HR, Picciani PHD, Silva K, Genre J, de Oliveira AG and do Egito EST, Understanding drug release data through thermodynamic analysis. *Mater* **10**:1-18 (2017).

Captions

Table 1. Codes of the produced membranes and specific area results.

Table 2. Fitting parameters of Korsmeyers-Peppas model on PVA20-HA-Ag and PVA30-HA-Ag membranes.

Table 1. Codes of the produced membranes and specific area results.

Nomenclature	PVA (% w/w)	HA (% w/w)	HA-Ag (% w/w)	Specific area $[\frac{m^2}{g}]$
PVA20	20	---	---	---
PVA30	30	---	---	---
PVA50	50	---	---	---
PVA20-HA	20	15	---	9.89
PVA30-HA	30	15	---	4.05
PVA50-HA	50	15	---	1.55
PVA20-HA-Ag	20	---	15	---
PVA30-HA-Ag	30	---	15	---
PVA50-HA-Ag	50	---	15	---

Table 2. Fitting parameters of Korsmeyers-Peppas model on PVA20-HA-Ag and PVA30-HA-Ag membranes.

Membrane	Model	R^2	Constants
PVA20-HA-Ag	Korsmeyer-Peppas	0.991	k=2.50 n=0.58
	Peppas-Sahlin	0.991	k_1=2.60 k_2=0.01 n=0.58
PVA30-HA-Ag	Korsmeyer-Peppas	0.998	k=0.45 n=0.79
	Peppas-Sahlin	0.999	k_1=0.44 k_2=4.3 * 10^{-4} n=0.79

Figure 1. a) SEM and b) TEM images of HA nanoparticles, c) SEM and d) TEM images of HA-Ag nanoparticles.
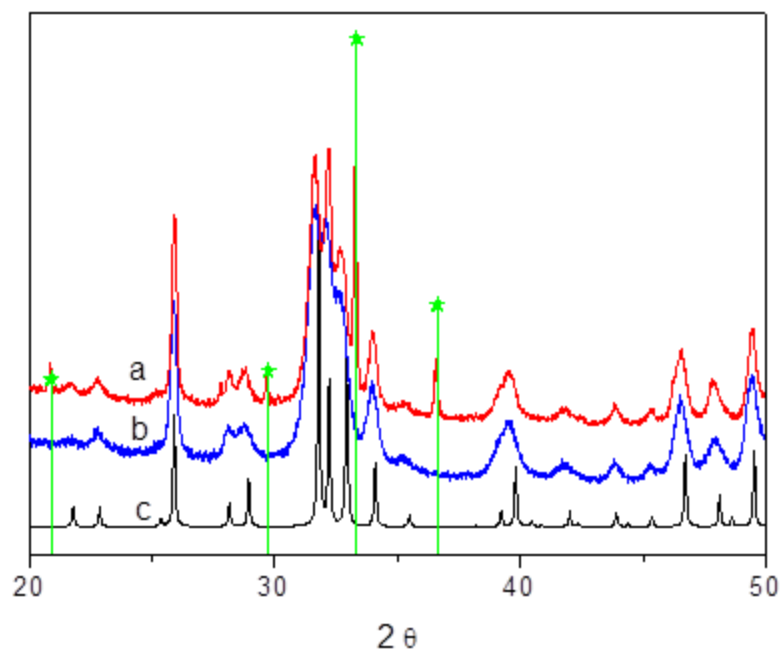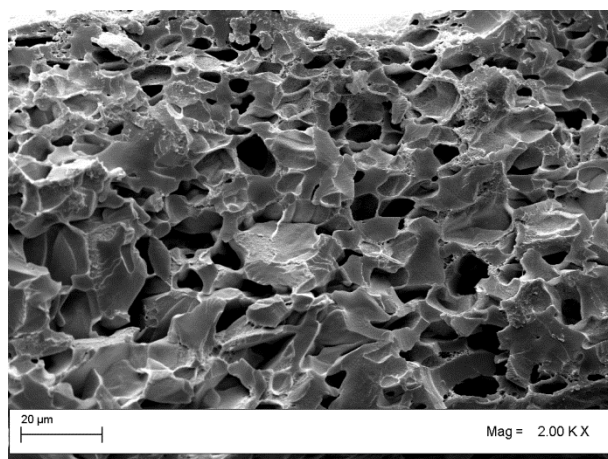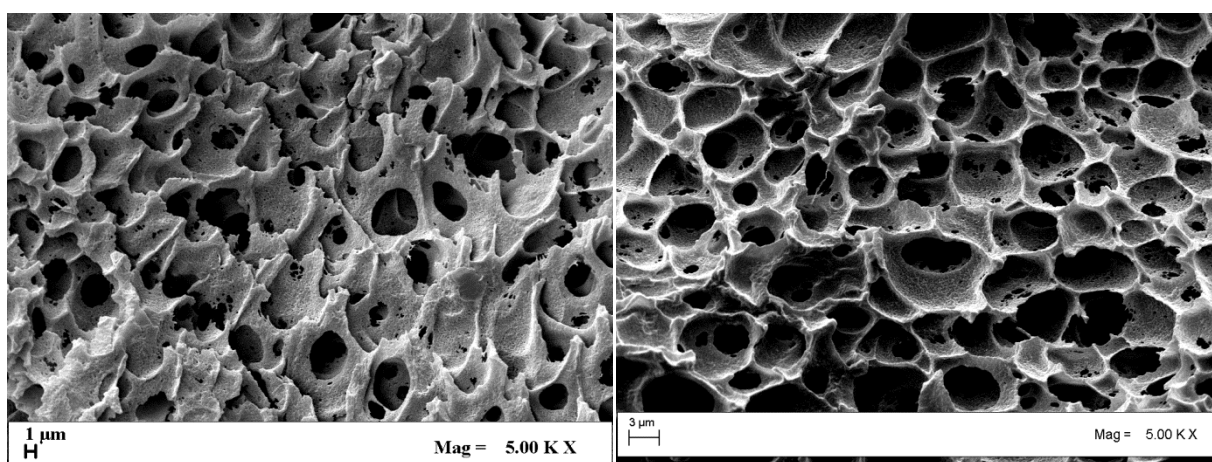
Figure 2. XRD of a) HA-Ag, b) HA-Ag nanoparticles and c) HA standard.

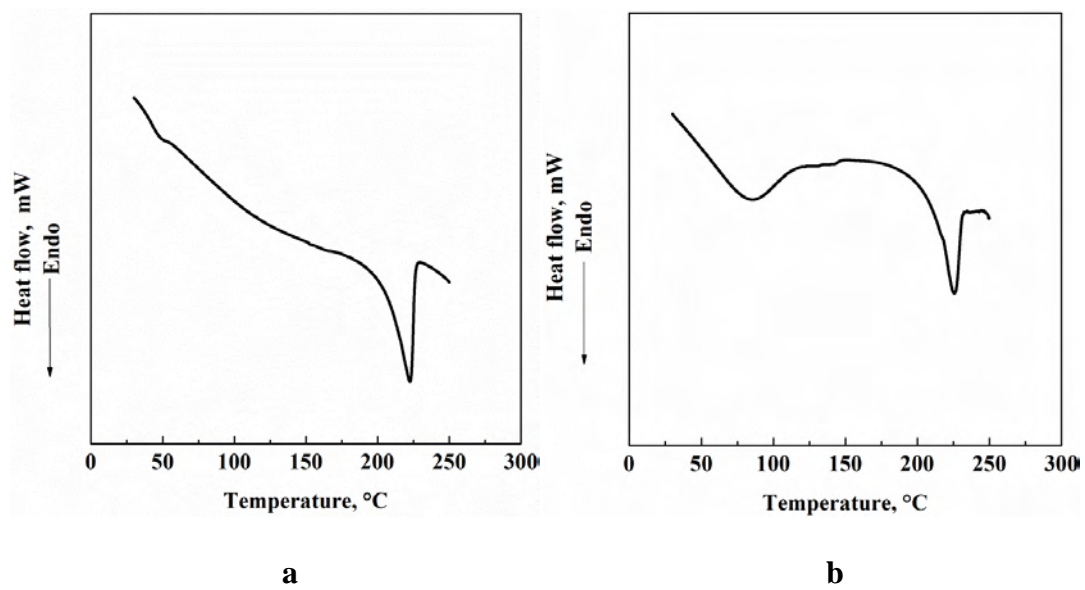**Figure 3.** SEM images of PVA20: a) 150 bar, 55 °C; b) 200 bar, 45 °C; c) 250 bar, 35 °C.

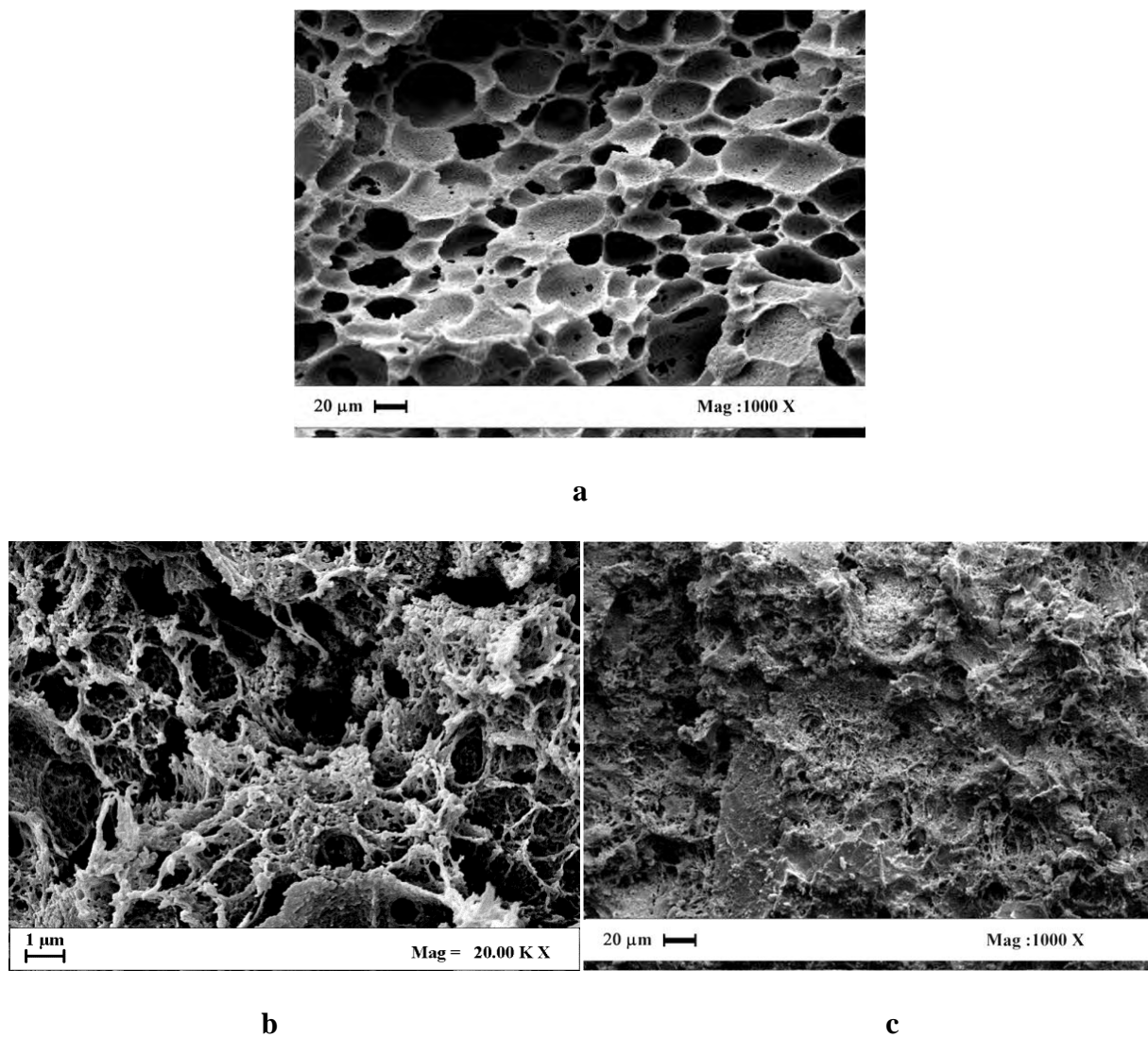**Figure 4.** DSC of (a) untreated PVA and (b) PVA20 membrane.

Figure 5. SEM images of: a) PVA20-HA, b) PVA30-HA and c) PVA50-HA membranes, obtained at 200 bar and 45 °C.
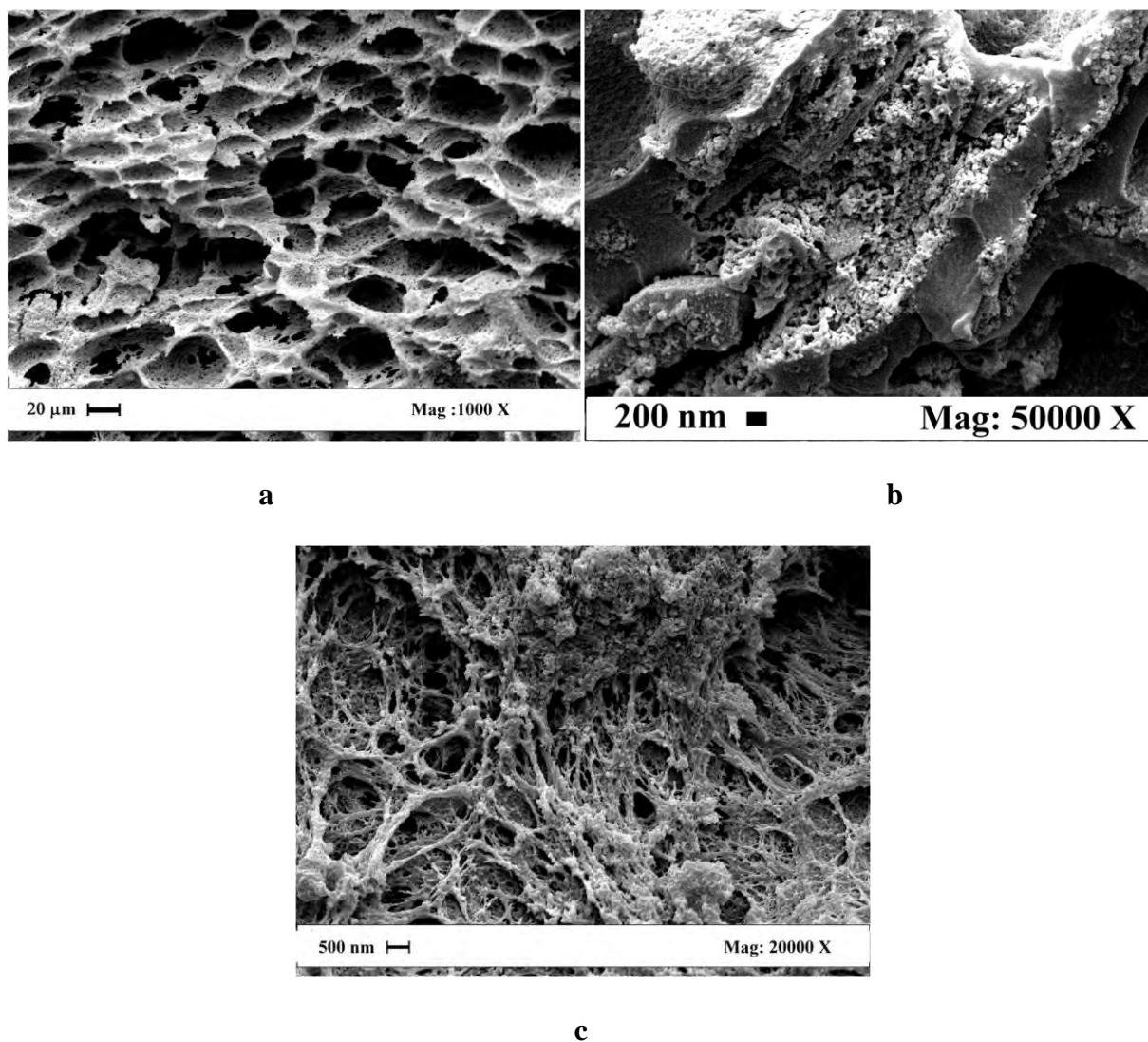
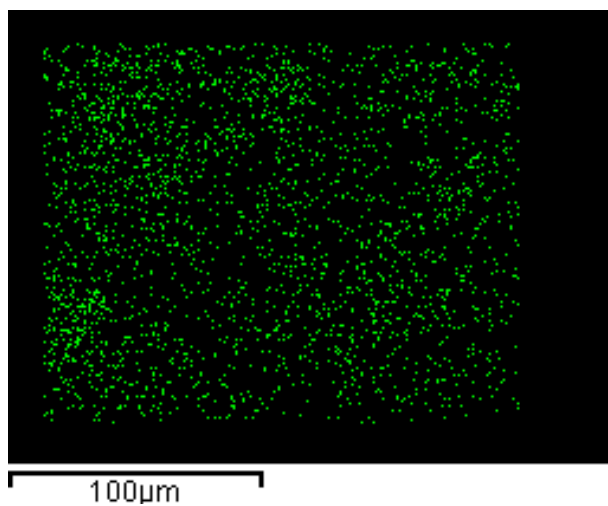**Figure 6.** SEM images of a) - b) PVA20-HA-Ag and c) PVA30-HA-Ag membranes, obtained at 200 bar and 45 °C.

Figure 7. EDX map of HA-Ag nanoparticles in a PVA20-HA-Ag membrane.

Figure 8. a) - b) Ag release from PVA20-HA-Ag and PVA30-HA-Ag plotted in terms of a) amount of Ag released and b) % of Ag released during 24 h; c) - d) comparison of the fitting models: c) PVA30-HA-Ag (Korsmeyers-Peppas: blu, Peppas-Sahlin: red) and d) PVA20-HA-Ag (Korsmeyers-Peppas: blu, Peppas-Sahlin: red) membranes during the first 8 h of release.

Figure 9. Bactericidal activity of HA-Ag nanoparticles at different concentrations on *E. coli* cultures after 24 h.

Figure 10. SEM images of A) and B) untreated, treated with C) and D) 1.8 ppm and E) and F) 5.4 ppm suspensions of HA-Ag nanoparticles.

Figure 11. Bactericidal results for PVA20-HA-Ag membranes against *E. coli* solid culture, liquid culture and the solid culture collection of 1 cm^2 around the membrane, for 24 h experiments.

Figure 1. a) SEM and b) TEM images of HA nanoparticles, c) SEM and d) TEM images of HA-Ag nanoparticles.

Figure 2. XRD of a) HA-Ag, b) HA-Ag nanoparticles and c) HA standard.

a

b

c

Figure 3. SEM images of PVA20: a) 150 bar, 55 °C; b) 200 bar, 45 °C; c) 250 bar, 35 °C.

Figure 4. DSC of (a) untreated PVA and (b) PVA20 membrane.

a

b

c

Figure 5. SEM images of: a) PVA20-HA, b) PVA30-HA and c) PVA50-HA membranes, obtained

at 200 bar and 45 °C.

Figure 6. SEM images of a) - b) PVA20-HA-Ag and c) PVA30-HA-Ag membranes, obtained at

200 bar and 45 °C.

Figure 7. EDX map of HA-Ag nanoparticles in a PVA20-HA-Ag membrane.

Figure 8. a) - b) Ag release from PVA20-HA-Ag and PVA30-HA-Ag plotted in terms of a) amount

of Ag released and b) % of Ag released during 24 h; c) - d) comparison of the fitting models: c)

PVA30-HA-Ag (Korsmeyers-Peppas: blu, Peppas-Sahlin: red) and d) PVA20-HA-Ag

(Korsmeyers-Peppas: blu, Peppas-Sahlin: red) membranes during the first 8 h of release.
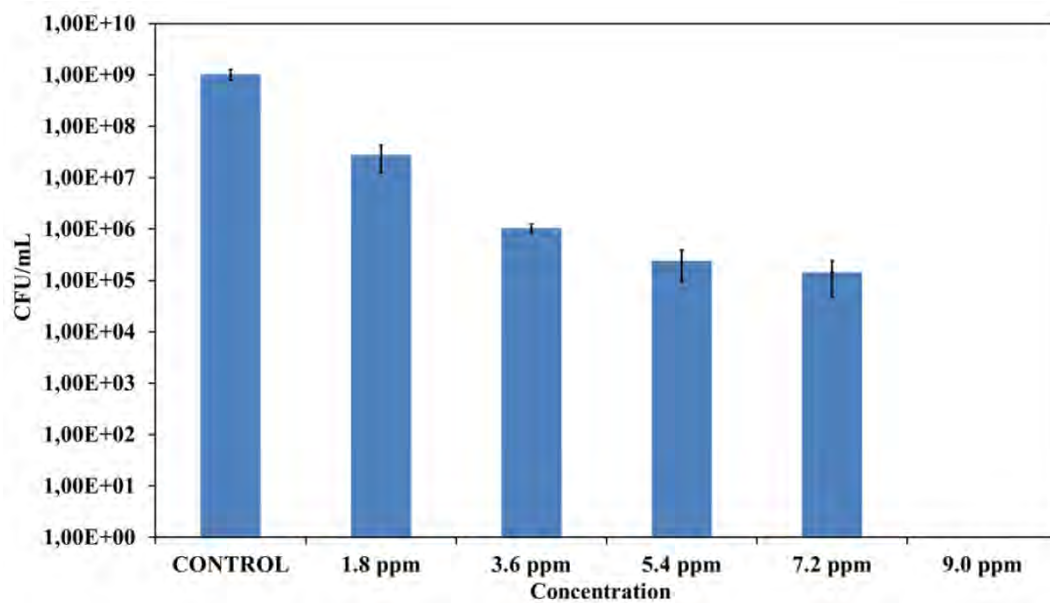
Figure 9. Bactericidal activity of HA-Ag nanoparticles at different concentrations on *E. coli* cultures after 24 h.
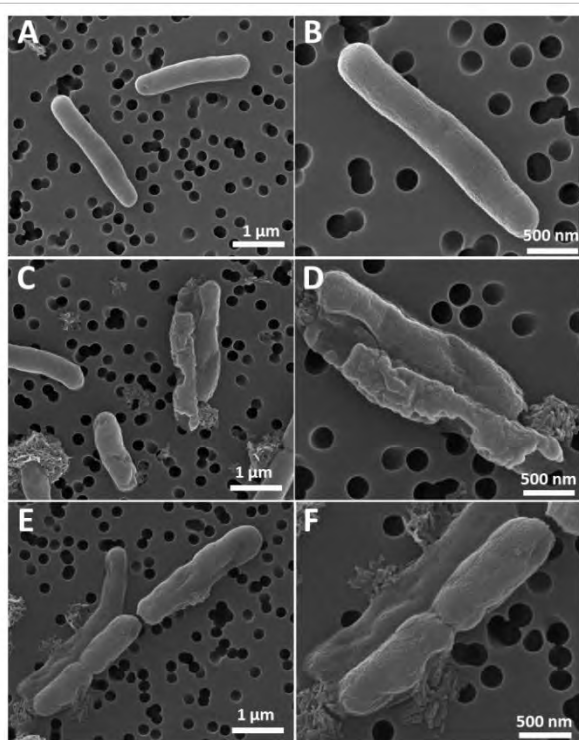
Figure 10. SEM images of A) and B) untreated, treated with C) and D) 1.8 ppm and E) and F) 5.4
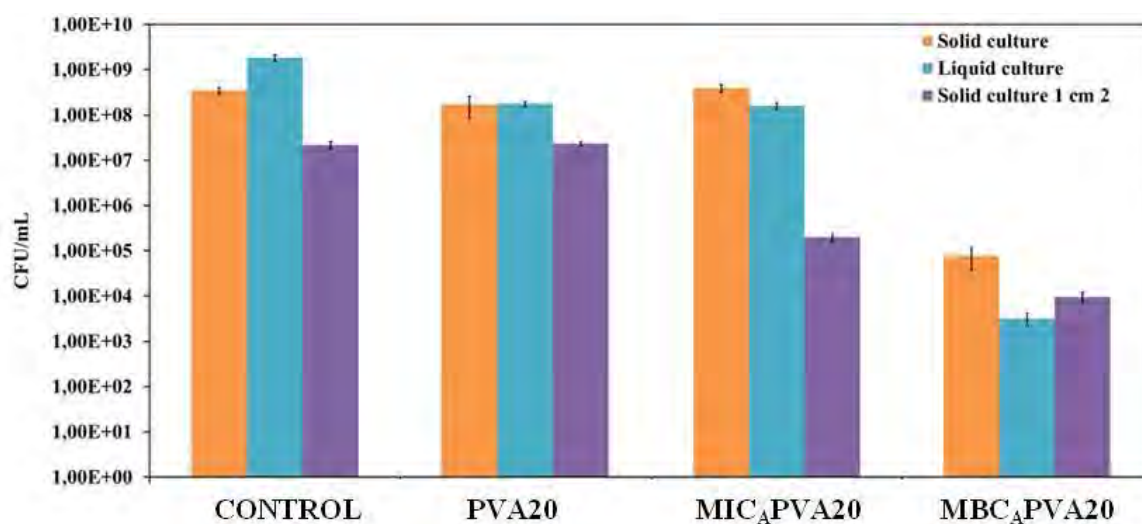
ppm suspensions of HA-Ag nanoparticles.

Figure 11. Bactericidal results for PVA20-HA-Ag membranes against *E. coli* solid culture, liquid culture and the solid culture collection of 1 cm^2 around the membrane, for 24 h experiments.